JOURNAL OF GEOPHYSICAL RESEARCH, VOL. 113, B06104, doi:10.1029/2007JB005502, 2008

Fundamental magnetic parameters from pure synthetic greigite (Fe_3S_4)

Liao Chang,[1] Andrew P. Roberts,[1] Yan Tang,[2] Brian D. Rainford,[3] Adrian R. Muxworthy,[4] and Qianwang Chen[2]

Received 15 November 2007; revised 15 November 2007; accepted 12 February 2008; published 13 June 2008.

[1] Pure ferrimagnetic greigite (Fe_3S_4) has been synthesized by reacting ferric chloride with thiourea and formic acid at 170°C. Sample purity was confirmed by X-ray diffraction, neutron diffraction and Mössbauer spectroscopy, coupled with magnetic measurements. Scanning electron microscope observations indicate clear cubo-octahedral and polyhedral crystal morphologies. The grain sizes are as large as 44 μm. Detailed low- and high-temperature magnetic measurements document the previously poorly known magnetic properties of greigite. The synthetic greigite samples are dominated by pseudo-single-domain and multi-domain behavior. The saturation magnetization (M_s) at room temperature is $\sim$59 Am^2kg^{-1} (3.13 μ_B per formula unit), which is higher than any value previously reported for greigite in the literature largely because of the high purity of this sample compared to others. No low-temperature magnetic transition has been detected; however, a local coercivity minimum is observed at around 130 K, which is probably associated with domain walls present in the studied samples. The high-temperature magnetic properties of greigite are dominated by chemical decomposition above around 250°C, which precludes determination of the Curie temperature, but our evidence indicates that it must exceed 350°C. On the basis of the Bloch spin wave expansion, the spin wave stiffness of greigite was determined for the first time as $\sim$193 meV·Å^2 from low-temperature M_s measurements, with the corresponding exchange constant J_{AB} of $\sim$1.03 meV.

Citation: Chang, L., A. P. Roberts, Y. Tang, B. D. Rainford, A. R. Muxworthy, and Q. Chen (2008), Fundamental magnetic parameters from pure synthetic greigite (Fe_3S_4), *J. Geophys. Res.*, *113*, B06104, doi:10.1029/2007JB005502.

1. Introduction

[2] Greigite (Fe_3S_4) is an iron thiospinel that was first formally discovered in lake sediments from California by *Skinner et al.* [1964]. Greigite was inferred to have the inverse spinel structure, the same as its iron oxide counterpart, magnetite (Fe_3O_4) [*Skinner et al.*, 1964]. Greigite has attracted considerable attention owing to its magnetic and electrical properties [e.g., *Coey et al.*, 1970; *Spender et al.*, 1972; *Vaughan and Tossell*, 1981; *Goodenough and Fatseas*, 1982; *Braga et al.*, 1988; *Vandenberghe et al.*, 1991; *Letard et al.*, 2005; *Pearce et al.*, 2006; *Rickard and Luther*, 2007]. In nature, greigite forms under anoxic, sulfate-reducing conditions and is being increasingly identified in anoxic marine and lake sedimentary systems and is now recognized as a widespread magnetic mineral [*Roberts and Weaver*, 2005, and references therein]. As a recorder of the ancient geomagnetic field and environmental processes, greigite can be important for paleomagnetic and environmental magnetic studies [e.g., *Snowball and Thompson*, 1988, 1990; *Snowball*, 1991; *Tric et al.*, 1991; *Roberts and Turner*, 1993; *Roberts et al.*, 1996, 2005; *Jiang et al.*, 2001; *Rowan and Roberts*, 2006; *Babinszki et al.*, 2007; *Ron et al.*, 2007; *Vasiliev et al.*, 2007]. Magnetotactic bacteria that produce greigite magnetosomes are also a potentially widespread source of greigite in nature [e.g., *Farina et al.*, 1990; *Mann et al.*, 1990; *Heywood et al.*, 1991; *Bazylinski et al.*, 1993, 1995; *Pósfai et al.*, 1998a, 1998b; *Kasama et al.*, 2006a, 2006b]. As a precursor to pyrite in the Fe-S system, greigite is significant in the pyritization process and in Fe-S geochemistry [e.g., *Berner*, 1984; *Benning et al.*, 2000; *Hunger and Benning*, 2007]. Greigite is therefore of interest in multiple disciplines, including geophysics, geochemistry, physics, biology and material science.

[3] The magnetic properties of greigite have been extensively studied. *Coey et al.* [1970] found that greigite is ferrimagnetic with the Néel spin configuration, which should have a net magnetic moment of $\geq$4 μ_B considering the spin-only values for the ionic moments. *Coey et al.*

[1]National Oceanography Centre, University of Southampton, European Way, Southampton, UK.
[2]Hefei National Laboratory for Physical Sciences at Microscale and Department of Materials Science and Engineering, University of Science and Technology of China, Hefei, China.
[3]School of Physics and Astronomy, University of Southampton, Southampton, UK.
[4]Department of Earth Science and Engineering, Imperial College London, South Kensington Campus, London, UK.

0148-0227/08/2007JB005502$09.00

[1970] could not account for the measured magnetic moment of only (2.2 ± 0.2) μ_B per formula unit (f.u.). They inferred that electron hopping occurs between high-spin ferric and ferrous iron in octahedral sites. *Spender et al.* [1972] presented two alternative band schemes to account for the semiconductor properties of greigite. *Goodenough and Fatseas* [1982] investigated the valence state of iron using the Mössbauer ^{57}Fe isomer shift. They argued that the reduction of the magnetic moment in greigite compared to that predicted for the Néel spin configuration might be due to a charge transfer from the S^{2-} $3p^6$ valence band to the octahedral site Fe $3d^6$ bands or to a delocalization of the Fe $3d$ electrons that form bonds with S atoms. *Braga et al.* [1988] made spin-polarized multiple-scattering calculations to investigate the electronic structure of greigite. Their calculations indicate that both the Fe^{2+} and Fe^{3+} high-spin configurations are expected in greigite and that the net magnetic moment per formula unit is ~3.02 μ_B/f.u. *Letard et al.* [2005] measured X-ray magnetic circular dichroic spectra on greigite and attributed differences in the spectra between greigite and magnetite to the presence of iron vacancies in greigite. Numerous other magnetic properties of greigite have also been reported in many paleomagnetic, rock magnetic and environmental magnetic studies [e.g., *Snowball and Thompson*, 1988, 1990; *Snowball*, 1991; *Hilton*, 1990; *Tric et al.*, 1991; *Hoffmann*, 1992; *Roberts and Turner*, 1993; *Fassbinder and Stanjek*, 1994; *Roberts*, 1995; *Dekkers and Schoonen*, 1996; *Roberts et al.*, 1996, 2006; *Sagnotti and Winkler*, 1999; *Dekkers et al.*, 2000; *Rowan and Roberts*, 2006].

[4] Despite the importance of greigite, and the many published studies of its magnetic properties, its fundamental magnetic characteristics remain relatively poorly known. For example, published values for the saturation magnetization (M_s) of greigite at room temperature are much lower than for magnetite (Table 1). This might be a result of difficulties in producing pure greigite samples. Greigite is an intermediate product in reactions that form pyrite (FeS_2) [*Berner*, 1984]. It therefore normally occurs in association with pyrite in natural environments. Natural greigite usually grows on the surface of other iron-bearing minerals [*Jiang et al.*, 2001; *Roberts and Weaver*, 2005], which makes it extremely difficult to separate magnetically from the other minerals and therefore to obtain pure natural samples. Although various methods have been proposed to synthesize greigite in the laboratory, including hydrothermal [*Yamaguchi and Katsurai*, 1960; *Uda*, 1965; *Yamaguchi and Wada*, 1969; *Dekkers and Schoonen*, 1996], anhydrous [*Nakazawa and Sakaguchi*, 1972], toluene-thermal [*Qian et al.*, 1999], solution-based hydrothermal [*Chen et al.*, 2005], and modified hydrothermal processes [*He et al.*, 2006], it is difficult to produce pure synthetic greigite because most procedures simultaneously produce other iron sulfides such as mackinawite and pyrite. Most greigite syntheses suffer either from back reaction on cooling back to room temperature or from the fact that greigite can easily react to pyrite in the presence of sulfidic sulfur because of its metastability. Additionally, synthetic greigite samples for which magnetic results have been reported in the literature usually have small particle sizes and/or poor crystallinity.

[5] Other magnetic properties of greigite also remain poorly understood. For example, the magnetic structure of greigite is not clear. Greigite, unlike magnetite, which undergoes a crystallographic phase transition at ~118 K [*Verwey*, 1939], has had no similar low-temperature transition detected [*Coey et al.*, 1970; *Spender et al.*, 1972; *Moskowitz et al.*, 1993; *Roberts*, 1995; *Chang et al.*, 2007]. Moreover, the easy axis of magnetization for greigite is the [100] crystallographic axis instead of the [111] crystallographic axis for magnetite at room temperature [*Yamaguchi and Wada*, 1970; *Heywood et al.*, 1991; *Bazylinski et al.*, 1993]. That is, the magnetocrystalline anisotropy is cubic with the first anisotropy constant positive, as is the case for metallic iron. To the authors' knowledge, the exchange constants and anisotropy constants have not been previously reported, although *Diaz-Ricci and Kirschvink* [1992] modeled various domain state configurations for greigite based on rough estimates of these parameters, assuming magnetite-like behavior. Thermal decomposition of greigite at elevated temperature has precluded determination of its Curie temperature (T_C).

[6] In this paper, we report magnetic results for hydrothermally synthesized pure greigite samples with good crystallinity produced using a new method [*Tang et al.*, 2007]. These greigite samples appear to be the purest samples yet synthesized and have much larger grain sizes than any previously reported. We have therefore used these samples to determine some of the fundamental magnetic parameters for greigite that were previously either unknown or poorly constrained.

2. Greigite Synthesis and Mineralogical and Magnetic Characterization

[7] Greigite samples were synthesized using a new hydrothermal method proposed by *Tang et al.* [2007] in which ferric chloride ($FeCl_3$) is reacted with thiourea (CH_4N_2S) and formic acid (HCOOH). Thiourea was used as a sulfur source to produce H_2S. All chemical reagents were analytical grade and purchased from Shanghai Chemical Reagents Company. To synthesize greigite, 3.0432 g of stoichiometric analytical grade $FeCl_3 \cdot 6H_2O$ was first dissolved in 100 ml of distilled water that had been purged with N_2 gas for at least half an hour to remove dissolved oxygen. 1.0465 g of thiourea was then added into the solution. After stirring for five minutes, 8.6 ml of formic acid was added into the mixed solution. The solution, which has pH below 4, was transferred into three Teflon-lined 60-ml stainless steel autoclaves. The hydrothermal reaction proceeded at 170°C for eight hours after sealing the autoclaves. Longer reaction times, e.g., 24 h, result in marcasite (FeS_2) contamination [*Tang et al.*, 2007]. During synthesis, N_2 was passed through the solution to prevent oxidation. After reaction, the autoclave was naturally cooled to room temperature. The filtered black precipitates were washed first with carbon disulfide to remove residual sulfur, and were then repeatedly washed alternately with distilled water and absolute ethanol. Finally, the material was dried in vacuum at 40°C for 4 h. A black powder was obtained.

[8] The recipe for synthesizing greigite proposed by *Tang et al.* [2007] is different from the traditional hydrothermal method in which a sodium sulfide solution is mixed with Mohr's salt (ferrous ammonium sulfate) [*Yamaguchi and Katsurai*, 1960; *Uda*, 1965; *Yamaguchi and Wada*, 1969;

Table 1. Summary of Grain Sizes and M_s Values Reported in the Literature for Greigite

Greigite Sample	Lattice Parameter/(Å)	Morphology and Grain Size	Domain State	M_s	Reference
Sediment	9.876	400–500 nm	?	?	*Skinner et al.* [1964]
Synthetic	9.90	30–50 nm	SP	24 Am^2kg^{-1}	*Uda* [1965]
Synthetic	9.85	spherical ~50 nm	?	?	*Yamaguchi and Wada* [1969]
Synthetic	9.86	10–15 nm	SP dominated	2.0 ± 0.3 μ_B/f.u.	*Coey et al.* [1970]
Synthetic	9.83–9.87	~9–14 nm	SP dominated	2.2 ± 0.3 μ_B/f.u.	*Spender et al.* [1972]
Synthetic	?	platelet, needle and disk-like <65 nm	?	?	*Horiuchi et al.* [1974]
Magnetosomes	?	75 nm	SD	?	*Mann et al.* [1990]
Magnetosomes	?	50–90 nm	SD	?	*Heywood et al.* [1991]
Sediment	9.88	<4–8 μm	PSD/MD	~20 Am^2kg^{-1}	*Hoffmann* [1992]
Synthetic	?	<150–400 nm	SP and SD	3–29 Am^2kg^{-1}	*Dekkers and Schoonen* [1996]
Magnetosomes	?	rectangular, arrowhead-shaped 30–120 nm	SD	?	*Pósfai et al.* [1998a, 1998b]
Synthetic	?	25 nm	?	?	*Qian et al.* [1999]
Synthetic	?	10 nm wide acicular, 100 nm irregular	SD	19.7 and 38.5 Am^2kg^{-1}	*Chen et al.* [2005]
Synthetic	?	plates, polyhedral, ~3 μm	PSD/MD?	28.6 and 44.7 Am^2kg^{-1}	*He et al.* [2006]
Magnetosomes	?	rectangular, random shapes	SD	?	*Kasama et al.* [2006a, 2006b]
Synthetic	9.872	cubo-octahedral, polyhedral 13 μm (<1–44 μm)	PSD/MD dominated	59 Am^2kg^{-1} 3.13 μ_B/f.u.	This study; *Chang et al.* [2007]

Dekkers and Schoonen, 1996]. In this new hydrothermal method, different iron and sulfur sources are used, and, after reaction, the autoclave is naturally cooled to room temperature rather than by quenching in cold water. Many studies suggest that quenching the reaction is essential to produce higher purity greigite samples [*Uda*, 1965; *Yamaguchi and Wada*, 1969; *Dekkers and Schoonen*, 1996]. Regardless, this hydrothermal method and others [*Qian et al.*, 1999; *Chen et al.*, 2005] consistently indicate that naturally cooling can also produce high quality greigite samples.

[9] The samples were immediately characterized by X-ray diffraction (XRD) analysis after synthesis using a Phillips X'pert X-ray diffractometer with high-intensity Cu-Kα radiation (λ = 1.54056 Å) at a scanning speed of 0.05°/s, with a 2θ range from 10 to 70° at the Department of Materials Science and Engineering, University of Science and Technology of China, Hefei, China. The samples were also characterized using scanning electron microscope (SEM) observations, which were made with a LEO 1450VP SEM, operated at 10–20 keV with an acceleration voltage of 17–20 pA at the National Oceanography Centre, Southampton (NOCS), University of Southampton, UK. Mössbauer spectra were measured at the Institute for Rock Magnetism (IRM), University of Minnesota, USA, both at variable temperatures and applied fields using a conventional constant acceleration drive and a ^{57}Co source. The applied magnetic field was parallel to the γ-ray path. A least-squares fit was used to decompose the spectra into sub-spectra that correspond to different distributions of hyperfine interaction parameters. The ^{57}Fe isomer shifts are relative to α-Fe measured at room temperature. Low- and high-temperature magnetic hysteresis loops and back-field magnetizations enabled determination of the coercive force (B_c), coercivity of remanence (B_{cr}), saturation remanent magnetization (M_r) and M_s using an automated Princeton Measurements Corporation vibrating sample magnetometer with low- and high-temperature attachments (to maximum applied fields of 1 T) at the IRM. M_s and zero-field-cooled (ZFC) and field-cooled (FC) magnetization measurements were made from 5 K to room temperature using a Quantum Designs Magnetic Properties Measurement System (MPMS). Hysteresis loops were measured between +5 T and −5 T using the MPMS at the IRM. Thermomagnetic measurements were made at the NOCS using a variable field translation balance (VFTB), with heating up to 700°C in air, an applied field of 27 mT and a heating/cooling rate of 10°C/min.

3. Results

3.1. Mineralogical Characterization

[10] After synthesis, the greigite samples were immediately subjected to XRD analysis to assess sample purity. Greigite is the only detectable phase (Figure 1). Rietveld refinement confirms that greigite has an inverse spinel structure with a cubic close-packed sulfur array (space group $Fd\bar{3}m$). The refined crystallographic lattice parameter is comparable to values reported in the literature (Table 1). The low background signal and the strong and narrow diffraction peaks also indicate good crystallinity, which is further confirmed by SEM observations (Figure 2). Greigite single crystals are clearly evident with variable morphology. However, most of the particles have equi-dimensional cubo-octahedral crystal habits. Elongation of the [111] or [100] crystallographic axes produces plate-like or prism-like crystals. Unusual polyhedral morphologies also occur, but they are rare. SEM observations indicate that this greigite sample has a range of grain sizes (Figure 3) [see also *Chang et al.*, 2007]. This sample is much coarser-grained than other synthetic and natural greigite samples described in the literature (Table 1). Because of the resolution limit of the SEM, the finest greigite particles could not be counted when determining the grain size distributions. This synthetic

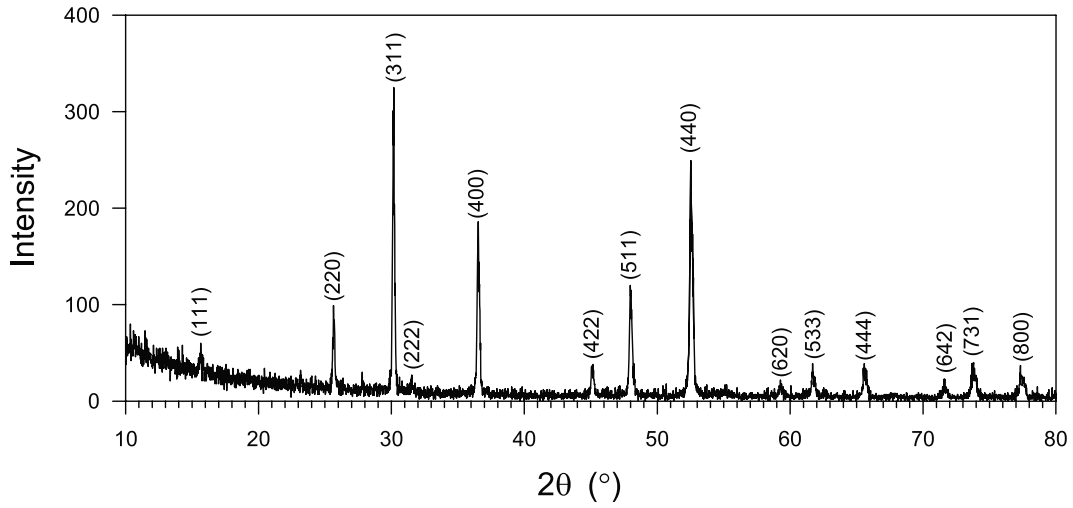

Figure 1. XRD pattern for the studied hydrothermally synthesized greigite sample at room temperature. The Miller indices of the main Bragg reflections are labeled.

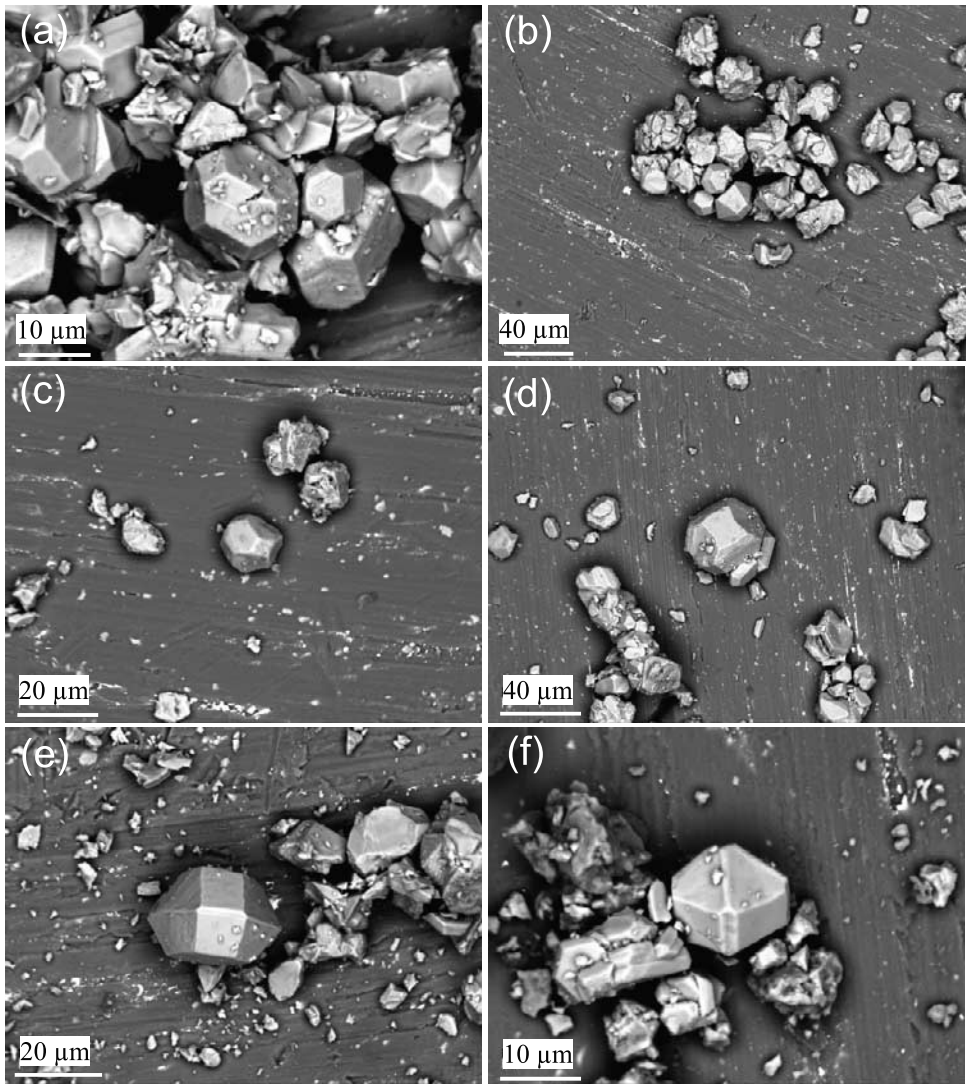

Figure 2. Backscattered electron images that illustrate the morphology and particle sizes of the studied synthetic greigite samples.

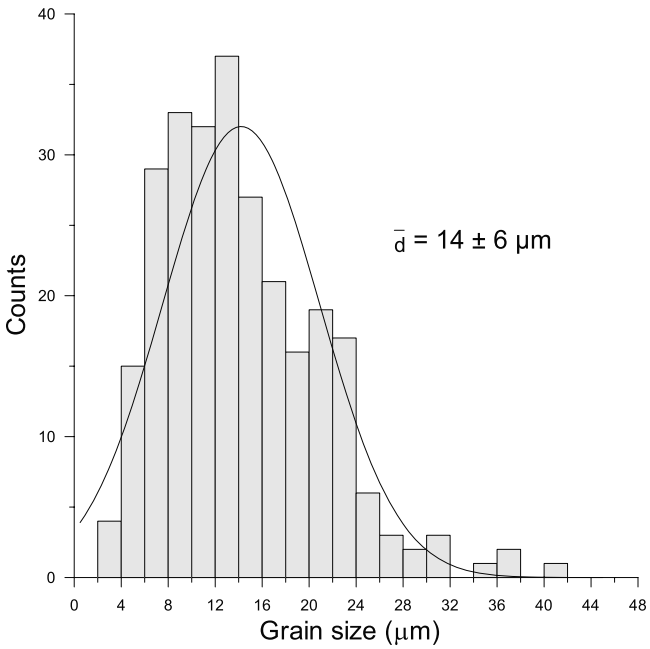

Figure 3. Histogram of the grain size distribution for the principal synthetic greigite sample studied in this paper, as determined from ~200 grain counts from SEM observations.

greigite sample is also made up of mechanically soft grains, as indicated in Figure 2 in which many crystals are physically crushed. This is not surprising as the hardness of greigite is in the 4–4.5 range (Mohr's scale) [*Radusinović*, 1966] (it should be noted that any literature estimate of the hardness of greigite will have been made from impure samples, so this estimate is probably too high because of the presence of mechanically harder minerals in an impure sample). The presence of extremely fine particles will affect the magnetic properties of the sample, especially by producing superparamagnetic (SP) behavior in ultrafine magnetic particles [*Néel*, 1949], which is evident in the Mössbauer and magnetic results described below.

[11] The purity of the studied greigite sample is further confirmed by other complementary measurements, e.g., neutron diffraction (L. Chang et al., Magnetic structure of greigite (Fe_3S_4) probed by neutron powder diffraction and neutron polarization diffraction, manuscript in preparation, 2008), Mössbauer spectroscopy and magnetization measurements. This confirmation is important because amorphous phases are not detectable using XRD. The synthesis of pure greigite samples in this study is significant because it is the first time that such a pure greigite sample has been synthesized. This makes it possible to rigorously determine some of the fundamental magnetic parameters for greigite for the first time.

3.2. Mössbauer Spectroscopy

[12] Mössbauer spectra were measured for the studied greigite samples both at room temperature and at low temperatures. The experimental spectra are shown in Figure 4 and the hyperfine interaction parameters, including the hyperfine field (B_{eff}) and the isomer shift (δ) obtained from analysis of the spectra, are listed in Table 2. At room temperature, the spectrum represents a superposition of a quadrupole doublet and two magnetic sextets. The two magnetic sextets are attributed to hyperfine interactions in the octahedral and tetrahedral sites in greigite. The quadrupole doublet is probably associated with thermally relaxed fine particles present in the measured sample. B_{eff} of the tetrahedral and octahedral sites for the studied greigite sample at room temperature is 31.2 and 31.5 T, respectively, while δ for the two sites is 0.29 and 0.53 mm/s, respectively. At 50 K, the Mössbauer spectrum is composed only of the two magnetic sextets that correspond to the two magnetic sublattices of greigite. The absence of the room temperature quadrupole doublet in the Mössbauer spectrum at low temperatures is an indication of SP behavior in the studied samples. At 4 K, the central quadrupole doublet disappears, while the two magnetic sextets are well defined in the Mössbauer spectrum. However, another small poorly defined magnetic sextet with higher B_{eff} (~48.4 T) is fitted to the Mössbauer spectrum at 4 K. This sextet is small and broad, which makes it difficult to determine its origin. However, it is probably associated with iron oxide, e.g., the two magnetic sextet peaks of magnetite or some solid solutions in the magnetite-maghemite (γ-Fe_2O_3) series [*Schmidbauer and Keller*, 2006]. The surface of greigite samples can become oxidized [e.g., *Letard et al.*, 2005; *Kasama et al.*, 2006b], which might be responsible for the observed small magnetic sextet with a high B_{eff} in the Mössbauer spectrum at 4 K. *Spender et al.* [1972] observed a much more pronounced magnetic sextet with a B_{eff} of ~47 T in the Mössbauer spectrum at 4.2 K. This suggests that the degree of surface oxidation in their samples was high, which is not surprising considering the large surface area to volume ratio for the small (~9 nm) synthetic greigite particles used in their study. Any surficial iron oxides only occur in small amounts in the greigite samples studied here, as indicated by the small and poorly fitted sextet. Its presence in such small quantities should not significantly affect our results.

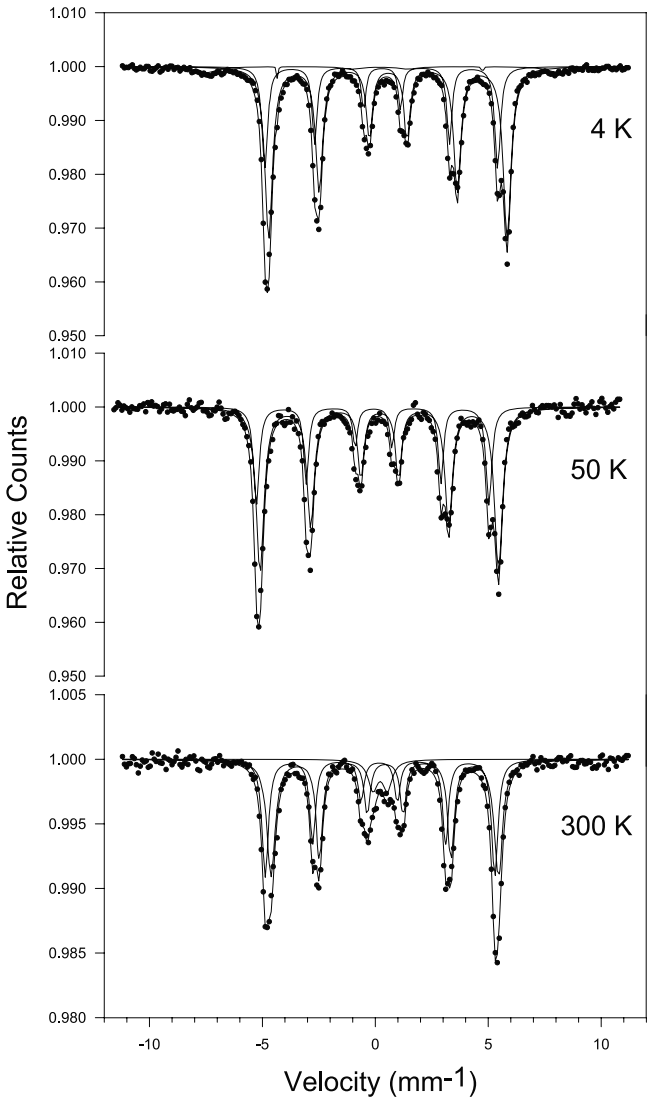

Figure 4. ^{57}Fe Mössbauer data (dots) for the studied greigite sample, measured with a ^{57}Co source at various temperatures (4 K, 50 K, and 300 K) in zero applied field. The curves represent the fittings for magnetic sextets and quadrupole doublets.

[13] Applying an external field to a magnetically split Mössbauer spectrum can change the magnetic field at the nucleus and affects the magnetic hyperfine interactions (Figure 5). The nuclear magnetic field (measured B_{eff}) can be expressed [*Greenwood and Gibb*, 1971] as:

$$B_{\text{eff}} = B_{\text{ext}} - DM + (4/3)\pi M + B_{\text{int}} = B_{\text{ext}} - DM + (4/3)\pi M + B_{\text{S}} + B_{\text{L}} + B_{\text{D}}, \quad (1)$$

where B_{ext} is the external applied field, $-DM$ is the demagnetizing field and $(4/3)\pi M$ is the Lorentz field, which are both small. B_{int} is referred to as the internal magnetic field, which is the sum of the Fermi contact term (B_{S}), the orbital term (B_{L}) and the dipole term (B_{D}). B_{S} originates from the unbalanced spin density of *s*-electrons at the nucleus. B_{L} arises from the orbital angular momentum of the ion. For high spin ferric compounds, this term is zero because ferric iron is an *S*-state ion, ^6S. B_{D} is the field produced at the nucleus by the arrangement of atomic moments throughout the crystal arising from the dipolar interaction of the nucleus with the spin moment of the atom. In cubic symmetry for transition elements, B_{D} is zero.

[14] The fact that B_{eff} at the octahedral site decreases, whereas B_{eff} at the tetrahedral site increases with increasing B_{ext} (Figure 6) indicates that B_{int} at the sublattices is aligned either parallel at the tetrahedral site or antiparallel to B_{ext} at the octahedral site, which reveals the ferrimagnetic nature of greigite. B_{eff} at the tetrahedral site has a smaller value (Table 2) due to the presence of Fe^{3+}. B_{eff} at both sites is nearly collinear with B_{ext} as predicted by equation (1). A crossover of the B_{eff} is observed at ~0.5 T (Figure 6), which is slightly different from previous observations [*Coey et al.*, 1970; *Spender et al.*, 1972].

3.3. Magnetic Properties

3.3.1. Saturation Magnetization and High-Field Behavior

[15] The studied greigite sample is magnetically soft, as suggested by a coercivity B_c of ~7–8 mT and a M_{rs}/M_s ratio of ~0.12 at room temperature. A hysteresis loop for the synthetic greigite sample at 5 K (Figure 7) quickly approaches saturation; however, it is not fully saturated even in a 5 T field. A contribution from spin waves may be responsible for the nonsaturation at high fields. Considering the nonsaturation at high fields, we use a conventional method to precisely determine the M_s. Magnetization is plotted against *1/B* (*B* is the applied field), and we extrapolate the magnetization to *1/B* = 0 to obtain $M(\infty)$ (Figure 8). For a range of greigite samples, the M_s at room temperature is determined to be ~59 Am^2kg^{-1} (3.13 μ_B/f.u.) for greigite (Table 1). Slightly higher values are

Table 2. Mössbauer Hyperfine Parameters for the Studied Greigite Samples Compared to Published Values for Greigite and Magnetite

		Octahedral Sites		Tetrahedral Sites	
Compounds	Temperature, K	Isomer Shift, mm/s	Hyperfine Field, T	Isomer Shift, mm/s	Hyperfine field, T
Greigite[a]	4	0.66	32.7	0.38	31.9
Greigite[a]	50	0.66	32.7	0.38	31.9
Greigite[a]	RT	0.53	31.5	0.29	31.2
Greigite[b]	RT	0.70	31.0	0.41	31.1
Greigite[c]	RT	0.53	31.3	0.28	31.3
Magnetite[b]	RT	0.82	46.2	0.43	49.4

[a]This study.
[b]*Coey et al.* [1970] and *Spender et al.* [1972].
[c]*Vandenberghe et al.* [1991].

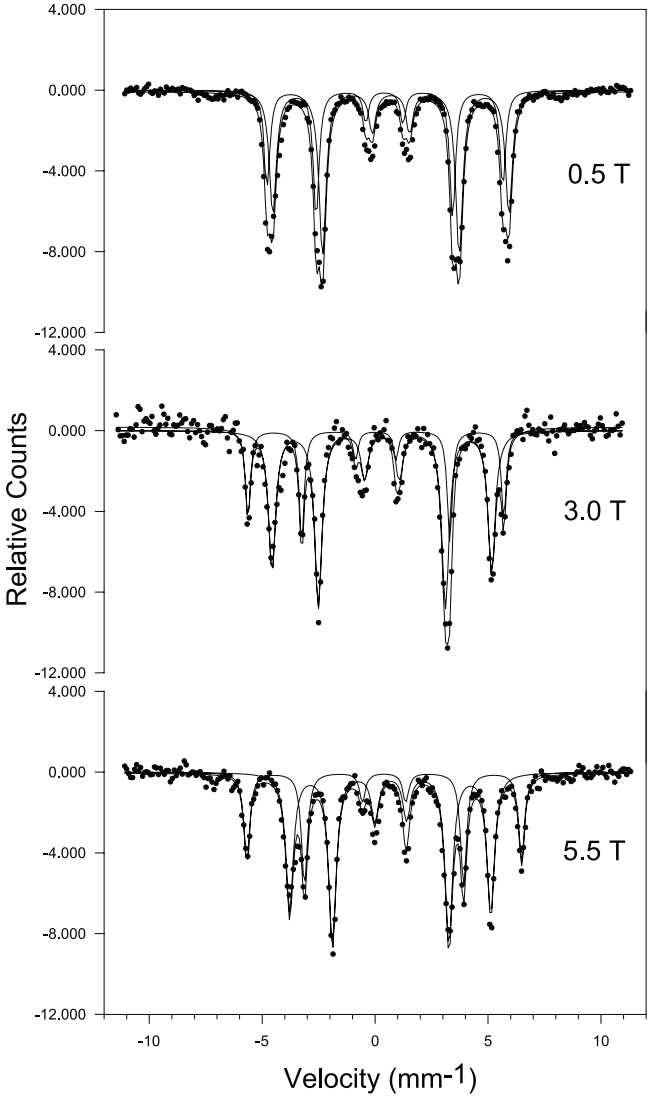

Figure 5. ^{57}Fe Mössbauer data (dots) and magnetic sextets (curves) for the studied greigite sample measured at 4 K under various applied fields (0.5 T, 3.0 T, and 5.5 T).

observed at lower temperatures because of decreased thermal agitation (Figure 8).

3.3.2. Low-Temperature Properties

[16] No low-temperature magnetic transitions were detected in any of the low-temperature measurements. This contrasts with magnetite, which undergoes a Verwey transition at 118 K [*Verwey*, 1939], and is consistent with previous reports for greigite [e.g., *Coey et al.*, 1970; *Spender et al.*, 1972; *Moskowitz et al.*, 1993; *Roberts*, 1995] and other low-temperature magnetic measurements for the same synthetic greigite samples [*Chang et al.*, 2007]. Variations in ZFC/FC magnetization curves measured in a 2 mT field are small, however, a clear maximum magnetization is observed at ~160 K in the ZFC curve (Figure 9), which is likely to indicate the presence of SP behavior in a fraction of the measured particles. M_s undergoes a 7.1% decrease from 5 K to room temperature (Figure 10) due to increased thermal fluctuations. The variation of B_c is small at low temperatures (Figure 11), as is often the case for

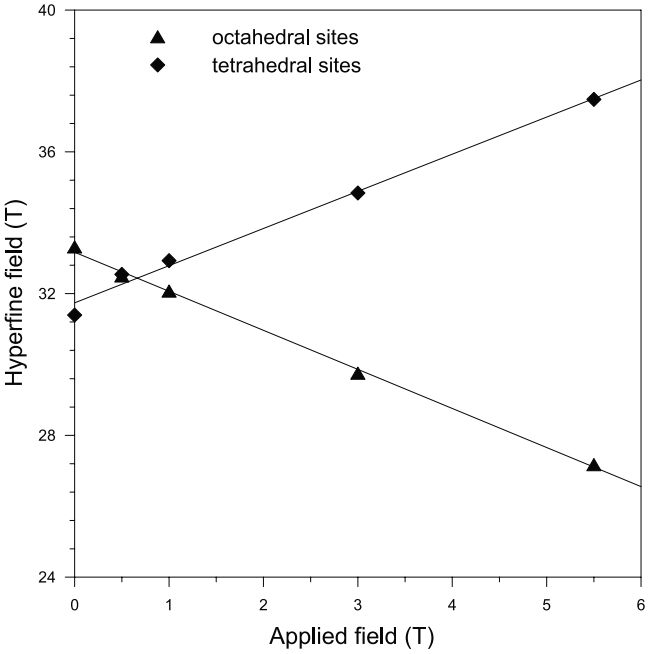

Figure 6. Field dependence of the sublattice hyperfine fields (solid triangles: octahedral sites; solid diamonds: tetrahedral sites).

natural single domain (SD) greigite samples [*Roberts*, 1995]. Despite the small change of coercivity at low temperatures, a clear local coercivity minimum was ob-

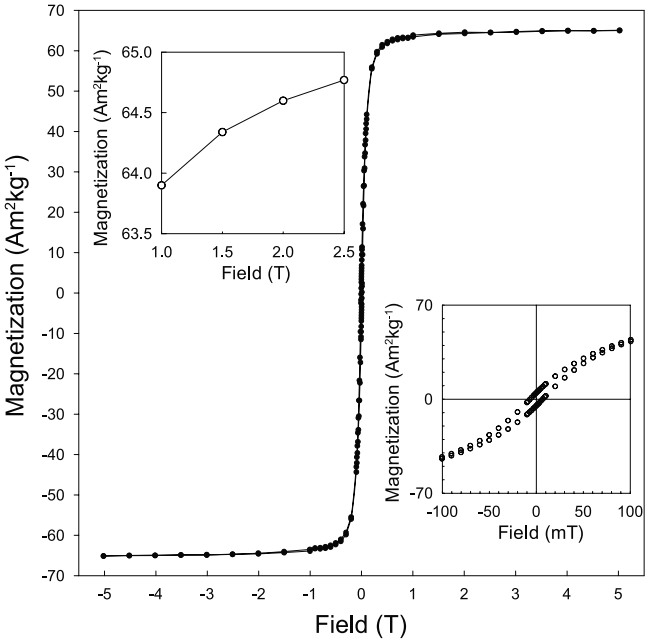

Figure 7. Field-dependence of magnetization for the studied greigite sample at 5 K. The insert on the bottom right-hand-side of the figure is an expansion of the central portion of the hysteresis loop, showing the coercivity and saturation remanence, while the insert on the upper left-hand-side of the figure contains the high-field approach to saturation magnetization.

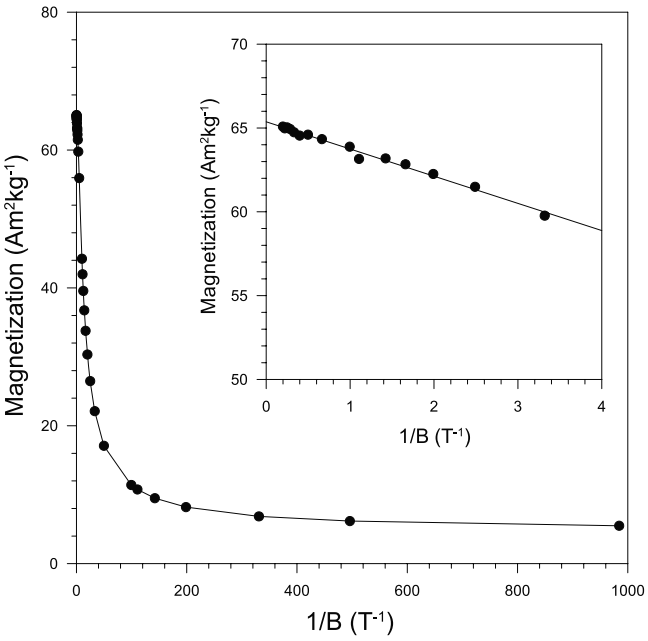

Figure 8. Magnetization versus $1/B$ for the studied synthetic greigite sample at 5 K. The insert is a horizontal expansion of the main figure at high fields, which indicates the approach to saturation. The same approach was used at room temperature, with extrapolation of the magnetization to $1/B = 0$ to obtain the M_s value for a range of samples.

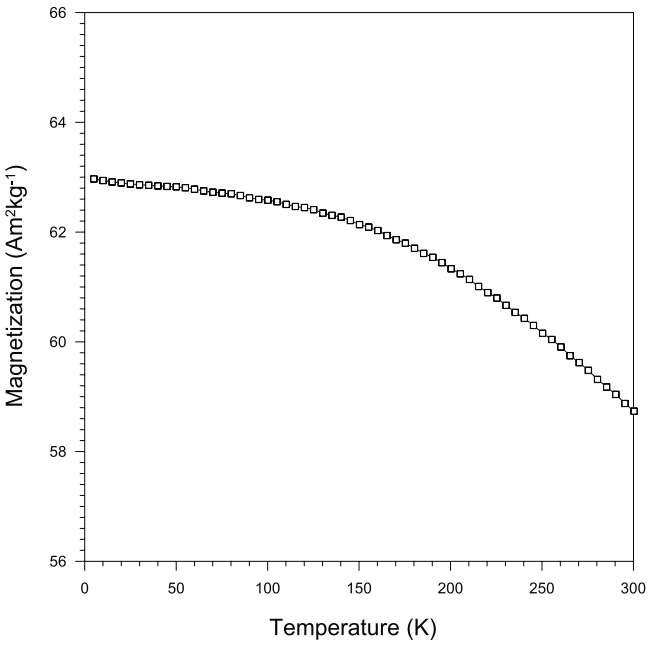

Figure 10. Low-temperature measurements of M_s for the studied greigite sample during warming from 5 K to 300 K measured in a field of 5 T. The M_s only decreases by 7.1% from 5 K to 300 K.

served at ~130 K. In order to check this property, we measured low temperature hysteresis loops for three synthetic greigite samples produced using the same hydrothermal method, which provides identical results (Figure 11). This confirms that the local coercivity minimum at ~130 K is a genuine magnetic property of greigite.

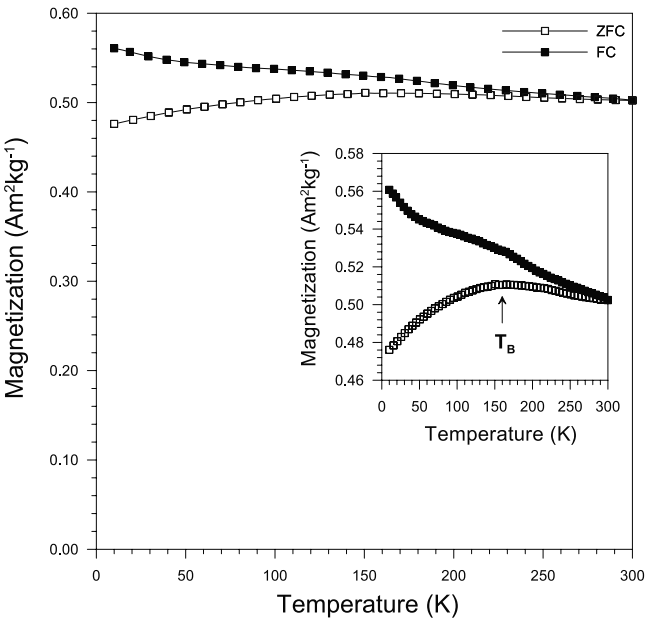

Figure 9. DC susceptibility versus temperature (at B = 2 mT) both in ZFC and FC conditions for the studied synthetic greigite sample. The insert is an expansion of the magnetization curves, which clearly indicates a blocking temperature at ~160 K due to the presence of fine grains with SP behavior.

3.3.3. High-Temperature Properties

[17] High-temperature hysteresis data (measured in air) reveal a significant break in slope at ~250°C (Figure 12), which indicates the onset of thermal decomposition of the studied greigite sample, as is widely known [e.g., *Krs et al.*, 1992; *Reynolds et al.*, 1994; *Roberts*, 1995; *Dekkers et al.*, 2000]. Both B_c and B_{cr} increase above 250°C, which indicates the formation of magnetically 'harder' phases. Thermal alteration has obscured efforts to determine the T_C of greigite.

[18] In order to investigate the possibility of a higher value for the T_C of greigite, we have measured high-temperature thermomagnetic curves for a particularly stable natural greigite sample from an iron sulfide nodule from the Valle Ricca section near Rome [cf. *Bracci et al.*, 1985; *Florindo and Sagnotti*, 1995; *van Dongen et al.*, 2007] (Figure 13). Studies of Italian greigite-bearing sediments have often suggested maximum unblocking temperatures for greigite of up to 380–410°C [e.g., *Florindo and Marra*, 1995; *Mattei et al.*, 1996; *Sagnotti and Winkler*, 1999; *Sagnotti et al.*, 2000]. The studied sample illustrates this behavior. Its thermomagnetic curve decreases sharply at ~400°C (Figure 13a). The curve eventually decreases to zero at the T_C of magnetite and is irreversible upon cooling. A peak at ~290°C is intermediate between the T_C of monoclinic pyrrhotite (Fe_7S_8) at 320°C [*Dekkers*, 1989] and that of hexagonal pyrrhotite (Fe_9S_{10}), which is only ferrimagnetic above ~200°C and which has a T_C of ~265°C [*Schwarz and Vaughan*, 1972]. During a second

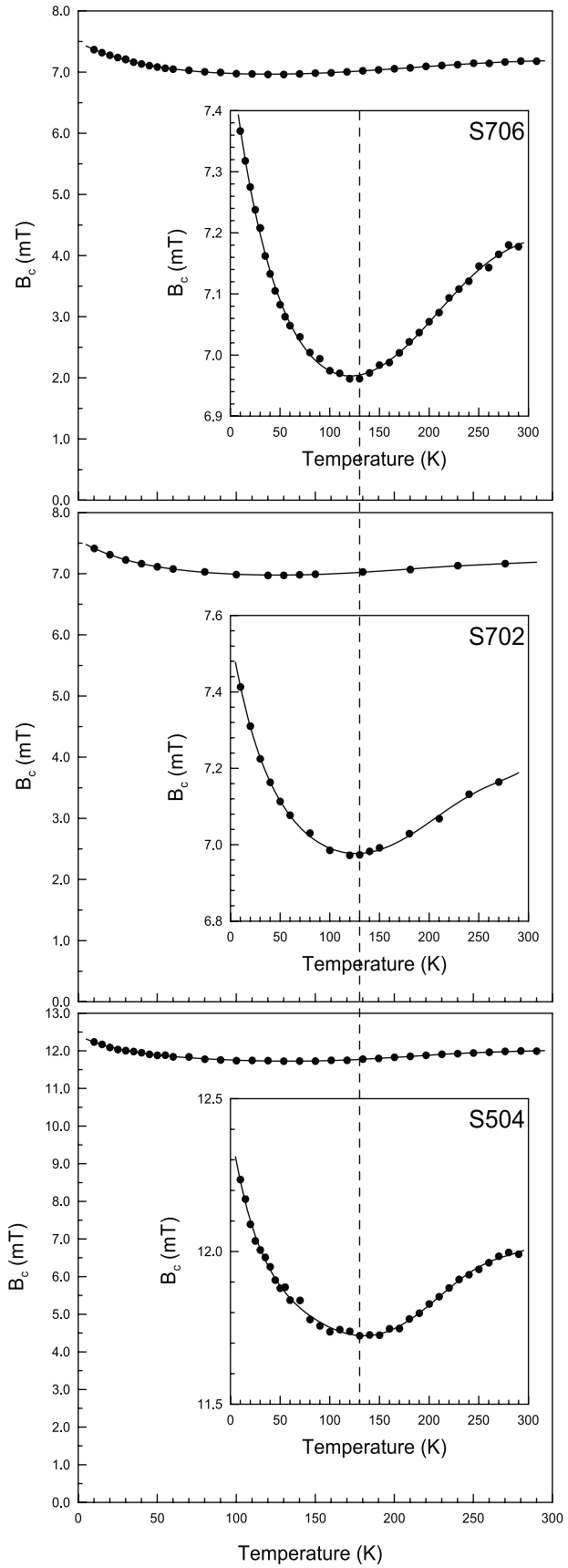

Figure 11. Temperature dependence of coercivity for three synthetic greigite samples at low temperatures. An apparent local coercivity minimum is observed at around 130 K for separate batches of the hydrothermally synthesized greigite.

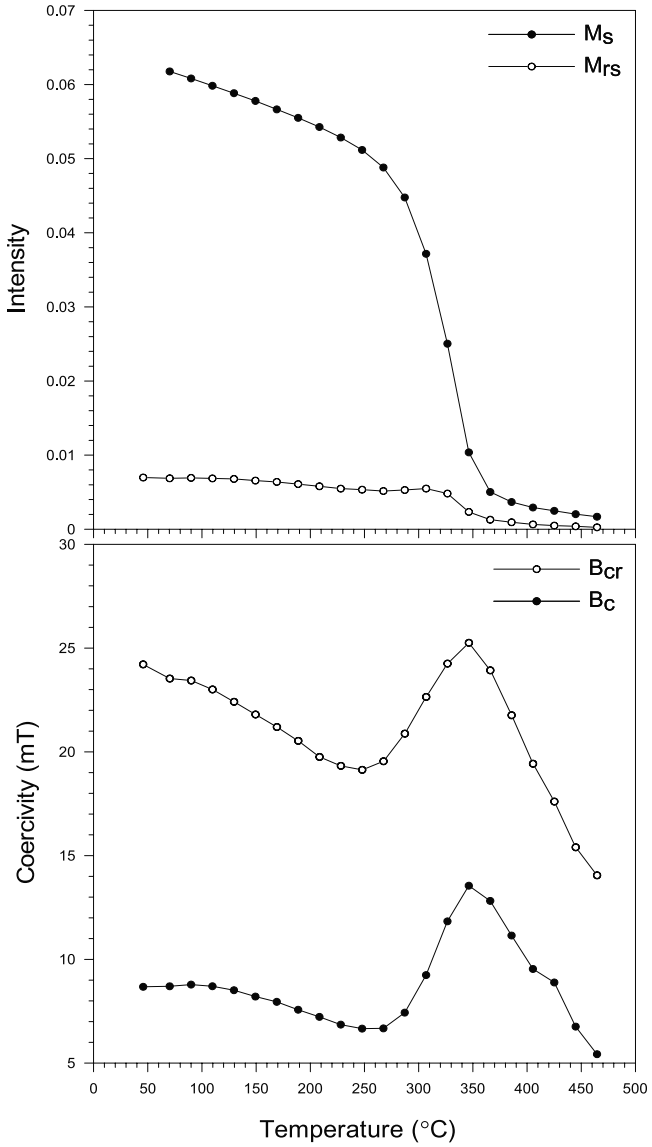

Figure 12. Temperature dependence of hysteresis parameters for the studied synthetic greigite sample at high temperatures. The break in slope of M_s at ~250°C indicates the onset of chemical decomposition of the synthetic greigite.

heating, this phase has clearly fully altered to form monoclinic pyrrhotite, as indicated by an inflection at 320°C during heating and a peak at this temperature during cooling (Figure 13b). Monoclinic pyrrhotite and magnetite appear to be the main magnetic phases present during the second heating run.

[19] In order to test whether the marked decay in magnetization at ~400°C in Figure 13a represents a T_C for a particularly stable greigite sample, a thermomagnetic run

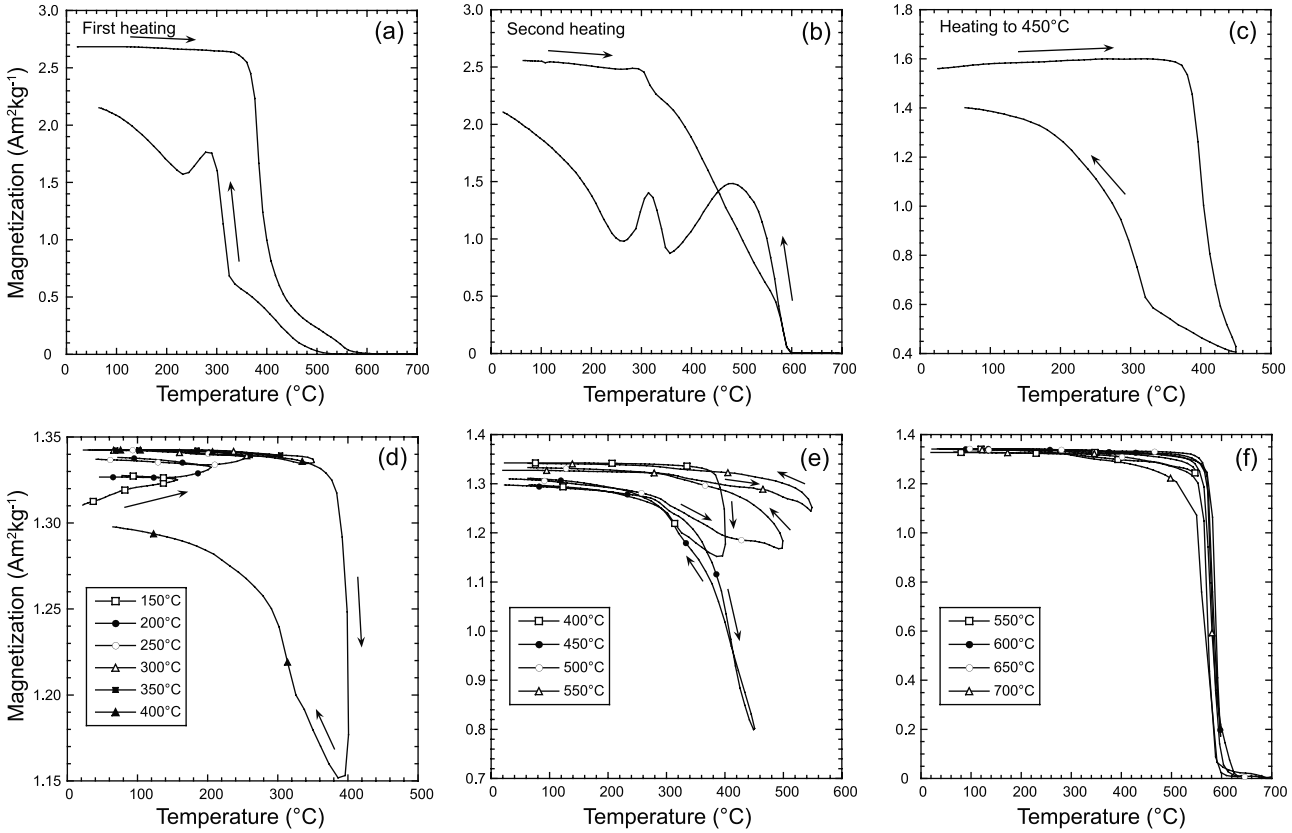

Figure 13. Thermomagnetic cycles for different subsamples of greigite from an iron sulfide nodule from the Valle Ricca section [cf. *Bracci et al.*, 1985; *Florindo and Sagnotti*, 1995]. (a) Thermomagnetic cycle up to 700°C and back to room temperature. (b) Second heating of the sample shown in Figure 13a. (c) Thermomagnetic cycle for a fresh sample up to 450°C. Thermal alteration is still evident in the cooling run for this sample. (d) Thermomagnetic cycles for another fresh sample up to progressively increasing maximum temperatures and back to room temperature, including maximum temperatures of 150°C, 200°C, 250°C, 300°C, 350°C, and 400°C. Note the expanded vertical scale in this subfigure. While slight increases in magnetization are evident up to 300°C, the 350°C curve is reversible, which suggests that the T_C for greigite must lie above 350°C. Thermal alteration is evident in the 400°C cycle. (e) Thermomagnetic cycles up to progressively increasing maximum temperatures and back to room temperature, including maximum temperatures of 400°C, 450°C, 500°C, and 550°C. Progressive thermal alteration is evident in each thermomagnetic cycle. (f) Thermomagnetic cycles up to progressively increasing maximum temperatures and back to room temperature, including maximum temperatures of 550°C, 600°C, 650°C, and 700°C. Each curve indicates that magnetite is present as the main magnetic alteration phase.

was measured on a sister sample to a maximum temperature of 450°C (Figure 13c) in an attempt to minimize thermal alteration. The data demonstrate that thermal decomposition of greigite occurs below 450°C for this sample. The fact that the high-temperature behavior of greigite is determined more by thermal alteration is evident from results for another sister sample that was subjected to successive thermomagnetic cycles at stepwise increasing maximum temperatures (Figures 13d-13f). The thermal cycling indicates progressive increases in magnetization (note the expanded vertical scale) up to about 250°C (Figure 13d). This increase could be similar to the increasing magnetic moments observed by *de Boer and Dekkers* [1998] when measuring samples in non-saturating fields. These authors stirred their samples between successive thermomagnetic runs to avoid such magnetic changes. We did not stir the samples between thermomagnetic runs, but we do not think that these changes indicate thermal alteration because further increases in magnetization are not observed above 250°C, and the 300 and 350°C cycles are reversible, which indicates that this sample is particularly stable with no discernible thermal alteration up to 350°C. Thermal alteration is clearly visible, however, in the 400°C cycle, where the heating and cooling curves are not reversible. An inflection in the cooling curve at 320°C suggests the formation of monoclinic pyrrhotite (Figure 13d). Pyrrhotite is clearly indicated in heating and cooling cycles up to 450°C, which is almost reversible (Figure 13e; note the larger vertical scale in this subfigure). Further thermal alteration, as indicated by irreversibility and increased magnetizations, is evident in the 500 and 550°C cycles. This newly formed phase is magnetite, as indicated by the reversible thermomagnetic curves with T_C of 580°C for cycles up to 600, 650, and 700°C (Figure 13f). While

thermal alteration is clearly a major determinant of the high-temperature magnetic properties of greigite, this sample is particularly stable, without thermal alteration (reversible thermomagnetic curves) up to 350°C, which indicates that the T_C of greigite exceeds 350°C.

3.4. Evaluation of the Exchange Constant for Greigite

[20] In ferrimagnets, information about the exchange energy is directly related to the spin wave stiffness. In the case of a ferrimagnetic spinel with two magnetic A and B sublattices, the spin wave stiffness has been shown to be [*Srivastava and Aiyar*, 1987]:

$$D = \left(2J_{AA}S_A^2 + 4J_{BB}S_B^2 - 11J_{AB}S_AS_B\right)a^2/|16(S_A - 2S_B)|, \quad (2)$$

where D is the spin wave stiffness, a is the lattice parameter, and J_{AA}, J_{BB}, and J_{AB} are the exchange integrals between the S_A and S_B spins on the A and B sublattices, respectively. As a first approximation, J_{AA} and J_{BB} can be considered to be negligible compared to J_{AB} [*Néel*, 1948].

[21] In a ferromagnetic system, a parabolic dispersion relation can be deduced from:

$$\hbar\omega = Dk^2, \quad (3)$$

where $\hbar$ is Planck's constant; ω and k are the frequency and wave vector of the magnon excitation. Several methods can be used to experimentally observe spin waves, e.g., inelastic neutron scattering, Brillouin scattering and spin wave resonance. Deriving information about the exchange energy is difficult without large single crystals to directly observe spin waves using inelastic neutron scattering. The lack of large single crystals of greigite means that these techniques cannot currently be applied to investigate the dynamic properties of spin waves in greigite. No useful information about the exchange energy of greigite exists in the literature.

[22] D can be deduced from the Bloch spin wave expansion of the spontaneous magnetization, which gives the $T^{3/2}$ term directly in terms of D, where T is temperature. This model is based on approximating the magnetic spin system as a system of harmonic oscillators. It has been shown that the spontaneous magnetization at low temperature is by approximation linear to the $T^{3/2}$ term using Bose-Einstein statistics. *Keffer* [1966] gives for a ferrimagnet:

$$M(T) = M_0\left[1 - \zeta(3/2)\Theta^{3/2} + L\right], \quad (4)$$

where ζ (3/2) = 2.612 is the Riemann zeta function, $\Theta = (g_{eff}\,\mu_B/M_0)^{2/3}k_BT/(4\pi D)$, $g_{eff} = (g_A\,S_A - g_B\,S_B)/|S_A - S_B|$ is the effective spectroscopic splitting factor g in ferrimagnets, and g_A and g_B are the g factors for sublattices A and B, respectively. L represents the higher order terms. M is the spontaneous magnetization, M_0 is the spontaneous magnetization at the ground state at 0 K, k_B is Boltzmann's constant, and μ_B is the magnetic moment in Bohr magnetons. A value of 2.0 can be taken for g_{eff}. By carefully measuring M_s for a large aligned sample, the spin wave stiffness can be obtained from the $T^{3/2}$ term of M_s using the spin wave model.

[23] We measured the low-temperature M_s for two synthetic greigite samples. The magnetization in a 5 T field at low temperature vs $T^{3/2}$ is plotted in Figure 14. M_s decreases with increasing temperature as thermal excitation of magnons increases. By expanding the magnetization to the next term, we get:

$$M(T) = M_0\left[1 - A_{3/2}\Theta^{3/2} + A_{5/2}\Theta^{5/2} + L\right]. \quad (5)$$

[24] Note that the coefficient of the $T^{5/2}$ term $A_{5/2}$ is positive, which could explain why M_s is concave upward

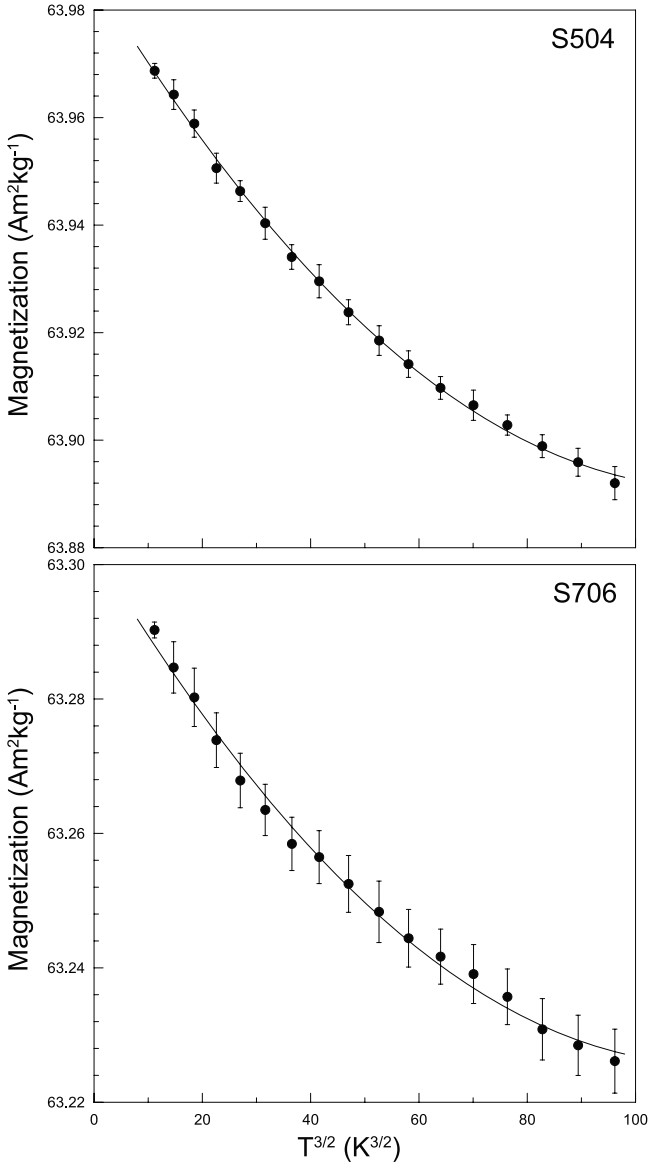

Figure 14. Magnetization in a field of 5 T versus $T^{3/2}$ for two field-cooled synthetic greigite samples at low temperatures. Decreased M_s indicates the presence of spin wave excitations as thermal excitation of magnons increases with increasing temperature. Bars on each data point represent the standard deviation of three magnetization measurements at each temperature. The solid line represents the second order polynomial fit to equation (5), which is used in the Bloch spin wave expansion to obtain the spin wave stiffness for greigite.

with increasing temperature (Figure 14). We apply the Bloch spin wave expansion and fit the low-temperature M_s data to a second degree polynomial of $T^{3/2}$ using equation (5). The corresponding D values for the two samples obtained from the M_s measurements are 182 meV·Å^2 and 205 meV·Å^2 with R^2 values of 0.9988 and 0.9943, respectively. The high R^2 values indicate strong polynomial regression of the low-temperature magnetization with respect to $T^{3/2}$. By using equation (2) and assuming values of S_A = 2.5, S_B = 2.25 and substituting a = 9.854 Å (Chang et al., manuscript in preparation, 2008), and as a first approximation ignoring J_{AA} and J_{BB}, we obtain the corresponding J_{AB} values of 0.97 meV and 1.09 meV for the two samples. The resulting effective exchange constant is $A = D \cdot M_s/(2g_{eff}\,\mu_B) = \sim 0.2 \times 10^{-11}$ J/m, which appears to be the first estimate of A for greigite.

4. Discussion

4.1. Fundamental Magnetic Parameters for Greigite

4.1.1. Saturation Magnetization

[25] We have demonstrated that the M_s of greigite is much higher than has been estimated in many previous studies (Table 1). The apparently low value of M_s for greigite in previous reports is not a genuine property of greigite, but is rather a result of sample impurity in these previous studies. Any magnetic and electronic models that are based on lower values of M_s for greigite should therefore be regarded with caution. The M_s value of 59 Am^{2}kg^{-1} (3.13 μ_B/f.u.) reported here is more likely to be the precise value for greigite because of the high purity of the studied sample. Neutron diffraction results for this sample enable unambiguous determination of the magnetic structure of greigite and reveal the tetrahedral and octahedral iron moments in greigite (Chang et al., manuscript in preparation, 2008). These analyses also indicate a consistent M_s value to that obtained from the magnetic measurements reported here, which is slightly higher than the value of ~3.02 μ_B/f.u. obtained by spin-polarized multiple-scattering calculations [*Braga et al.*, 1988].

[26] Assuming that the magnetic structure of greigite is identical to that of magnetite and considering the different atomic weight of O and S, the M_s for greigite at room temperature would be ~70 Am^{2}kg^{-1} (~4 μ_B/f.u.), which is slightly higher than the value obtained in this study. Neutron diffraction also indicates that the net magnetic moment of the two sublattices in greigite is slightly lower than for magnetite (Chang et al., manuscript in preparation, 2008), which would explain why M_s is slightly lower than for magnetite. Nevertheless, the value determined here is much closer to that of magnetite than any previously published estimates, which has important implications for the electronic and magnetic structure of greigite. Accurate determination of M_s is therefore important for understanding the magnetic properties of greigite, its magnetic structure, cation distribution and coordination. A precise value of this parameter is also crucial for micromagnetic and other modeling of greigite.

4.1.2. Mössbauer Parameters

[27] Previous Mössbauer spectra for greigite have been measured on poorly crystalline, non-stoichiometric fine-grained synthetic samples or impure natural samples. The hyperfine parameters obtained in this study are comparable to those reported in the literature (Table 2); however, they are probably more reliable because the sample studied here is purer than any other previously analyzed sample. Compared to magnetite, the B_{eff} is much lower for greigite, which is probably caused by a strong increased covalency effect in greigite. δ for the tetrahedral site is low (Table 2), which indicates that the tetrahedral iron is dominantly ferric [*Coey et al.*, 1970; *Vandenberghe et al.*, 1991]. δ for the octahedral sites of 0.53 mm/s at room temperature (this study) suggests that the valence of these irons might be either high-spin ferrous or intermediate between ferrous and ferric [*Spender et al.*, 1972]. B_{eff} at both the tetrahedral and octahedral sites increases at low temperatures, with respective values of 31.9 and 32.7 T at 4 K, which is consistent with the study of *Vandenberghe et al.* [1991]. However, they also observed a cross-over of B_{eff} values for tetrahedral and octahedral sites at ~290 K and obtained nearly equal B_{eff} values at room temperature. Our B_{eff} value for the octahedral sites is higher than for the tetrahedral sites below room temperature, which indicates that the effective spin for the octahedral sites is higher than for the tetrahedral sites. Unlike *Coey et al.* [1970] and *Spender et al.* [1972], who found almost the same values of B_{eff} for the two sites when extrapolating the two patterns to zero field, our study indicates a cross-over of values at ~0.5 T and a higher value for the octahedral sites at zero field.

4.1.3. Exchange Constant

[28] First estimates of the exchange constant J_{AB} (mean value of ~1.03 meV) and of the mean value of the spin wave stiffness (D = ~193 meV·Å^2) provided in this study give useful information for greigite. The exchange energy of magnetite has been extensively studied to verify the spin wave theory. However, variable measured values have been obtained for the exchange constant for magnetite with different approaches, e.g., inelastic neutron scattering (D = ~443 meV·Å^2) [*Brockhouse and Watanabe*, 1963], low-temperature specific heat capacity measurements (D = ~60 meV·Å^2) [*Kouvel*, 1956], (D = ~318 meV·Å^2) [*Kenan et al.*, 1963] and low-temperature M_s measurements (D = ~270 meV·Å^2) [*Aragón*, 1992]. The inconsistency is probably due to the complex nature of spin waves in ferrimagnetic spin arrangements [*Srivastava and Aiyar*, 1987]. Direct observations of spin waves, e.g., determination of the dispersion relations for the acoustic and optic magnon modes by inelastic neutron scattering on single crystals, are needed for greigite to check the estimated value of the exchange constant obtained here and to check the reliability of this approach.

4.1.4. Curie Temperature?

[29] Greigite is chemically unstable at high temperatures, therefore high temperature magnetic measurements often reveal chemical decomposition rather than the T_C [*Krs et al.*, 1992; *Reynolds et al.*, 1994; *Roberts*, 1995; *Dekkers et al.*, 2000]. This makes it difficult to determine T_C for greigite, which remains unknown despite variable estimations reported in the literature. *Spender et al.* [1972] obtained an estimate for T_C of 333°C by extrapolating thermomagnetic curves to high temperatures, although it is likely that this estimate was affected by thermal alteration. *Vandenberghe et al.* [1991] made Mössbauer spectroscopic measurements up to 207°C and extrapolated B_{eff} of iron in

tetrahedral sites to obtain a T_C value of at least 800 K (527°C) for greigite. No other corroborating data are available to indicate whether this is a reasonable inference. *Roberts* [1995] found a break in slope of the trend for all hysteresis parameters at 595 K (322°C). This break must mark the lower limit of the unblocking temperature range at which thermal energy begins to overcome the magnetocrystalline anisotropy for greigite. Evidence presented here (Figure 13) indicates that T_C is likely to exceed 350°C in greigite. This is in disagreement with a T_C of ~320–330°C that is often incorrectly cited for greigite [e.g., *Opdyke and Channell*, 1996; *Dunlop and Özdemir*, 1997]. The major break in slope at 250°C for the plotted hysteresis parameters (Figure 12) for the studied greigite sample is lower than T_C estimates from the literature, which indicates that the synthetic samples studied here decomposed after heating at and above 250°C.

4.2. Magnetic Properties

4.2.1. Dominant Pseudo-Single-Domain (PSD) and Multi-Domain (MD) Behavior

[30] The grain size of the studied synthetic greigite sample is in the micron to tens of microns range (Figure 3), which is large enough for PSD and MD behavior to dominate the sample [*Hoffmann*, 1992; *Chang et al.*, 2007]. The coercivity of this synthetic sample is much lower than in most natural sedimentary greigite samples, which are often found in the SD state and therefore have much higher coercivities [*Roberts*, 1995; *Roberts et al.*, 2006], although SP greigite is also common in many reducing environments [*Rowan and Roberts*, 2006]. The low coercivity in the studied synthetic greigite samples might therefore be caused by either MD or SP behavior; however, low-temperature hysteresis measurements do not indicate substantial magnetic blocking as expected for SP grains (Figure 11). Detailed analysis of the magnetic behavior of the studied synthetic greigite sample confirms that it is dominated by PSD/MD behavior [*Chang et al.*, 2007].

4.2.2. Presence of SP Behavior

[31] Although the studied greigite samples are dominated by large grains (Figures 2 and 3) with PSD/MD properties, restricted SP behavior is also observed in magnetic and Mössbauer measurements. ZFC/FC susceptibility measurements for one studied greigite sample indicate a clear maximum in magnetization at ~160 K in the ZFC curve (Figure 9). This is probably the mean blocking temperature of fine particles in the measured greigite sample. This interpretation is supported by Mössbauer data (Figure 4). In the ordered magnetic hyperfine spectra, the six-line hyperfine spectrum would collapse with decreasing relaxation time caused by spin-wave time-averaging [*Greenwood and Gibb*, 1971]. If the fluctuation rate is slow compared to the precession frequency of the nucleus in the field, the full six-line pattern is observed. If the fluctuation rate is extremely rapid, the nucleus will only respond to the time-averaged field which is zero and a symmetric quadrupole pattern will be seen. At room temperature, the central doublet (Figure 4) is probably due to thermally relaxed fine particles, which is confirmed by low-temperature Mössbauer measurements. The central quadrupole doublet present at room temperature disappears at 4 K and 50 K (Figure 4); fine particles are blocked and contribute to the observed sextets. Fine greigite particles therefore appear to be responsible for the SP properties that produced the quadrupole doublet in room temperature Mössbauer spectra. The origin of these fine particles is not clear. They may have been produced during synthesis, although they could also be small fragments that were produced by damaging the large, soft crystals during sample preparation.

4.2.3. Low-Temperature Coercivity Minimum

[32] A low-temperature coercivity minimum occurs in all of the studied greigite samples (Figure 11). No such coercivity minimum has been reported before [e.g., *Spender et al.*, 1972; *Moskowitz et al.*, 1993; *Roberts*, 1995]. However, previous studies were predominantly based on SD or SP greigite samples, while the observed local coercivity minimum occurs in PSD/MD greigite, and is probably related to the presence of magnetic domains (i.e., domain re-ordering). Nevertheless, we are currently unable to provide a detailed explanation for this local coercivity minimum.

4.3. Comparison of Greigite With Magnetite

[33] It is useful to compare greigite and its oxide equivalent, magnetite (Fe_3O_4). These two minerals have a similar chemical composition and share the same inverse spinel crystal structure [*Skinner et al.*, 1964]. Magnetite should therefore be a reasonable analog for understanding the magnetism of greigite. The magnetic properties of magnetite have been well established for decades [*Dunlop and Özdemir*, 1997, and references therein], but the fundamental magnetic parameters for greigite are still poorly known. Despite expected similarities between the two phases, their magnetic properties are different in many aspects. (1) *Saturation magnetization.* In the literature, the M_s of greigite is often suggested to be less than one-third that of magnetite (Table 1). We have demonstrated that the M_s for greigite at room temperature is about 59 Am^2kg^{-1}, which is lower than the value of ~90–92 Am^2kg^{-1} for magnetite even when considering the difference in atomic weight of O and S atoms (which converts to ~70 Am^2kg^{-1}). Neutron diffraction results verify that the M_s for greigite is slightly smaller than that of magnetite (Chang et al., manuscript in preparation, 2008). (2) *Low-temperature magnetic transition*. Despite similarities in the chemical composition and crystal structure of these two spinels, no low-temperature magnetic discontinuities are observed for greigite, as indicated in this and in other studies [*Coey et al.*, 1970; *Spender et al.*, 1972; *Vandenberghe et al.*, 1991; *Moskowitz et al.*, 1993; *Roberts*, 1995; *Dekkers et al.*, 2000]. (3) *Easy axis of magnetization*. In magnetite, the [111] crystallographic axis is the easy axis of magnetization at room temperature. However, the easy axis of magnetization for greigite has been shown to be the [100] crystallographic axis, as determined by *Yamaguchi and Wada* [1970] using electron diffraction. This observation has been confirmed by electron microscopic observations of bacterial greigite magnetosomes [e.g., *Heywood et al.*, 1991; *Bazylinski et al.*, 1993]. (4) *Exchange energy.* Our estimated exchange constant for greigite is lower than that of magnetite. This could be a result of the replacement of oxygen by sulfur in the spinel crystal lattice in greigite. This is likely to affect the superexchange coupling between iron in the octahedral and tetrahedral sites. These properties and others demonstrate

some intrinsic differences between the fundamental magnetic parameters of two spinels, magnetite and greigite. Some of these must reflect fundamental differences, e.g., in electronic structure, which demonstrate that considerable caution must be taken when making comparisons between these two inverse spinel minerals.

5. Conclusions

[34] Pure synthetic greigite samples were produced with a new hydrothermal method. XRD, magnetic, Mössbauer spectroscopy and neutron diffraction measurements confirm sample purity. SEM observations demonstrate the crystallinity and morphology of individual greigite crystals, most of which are cubo-octahedral, with grain sizes up to 44 μm. These samples have the largest mean particle size of any synthetic or natural greigite sample described in the literature. Some crystals are elongated, with plate-like or prism-like crystals being the dominant morphologies.

[35] The following magnetic properties have been determined for greigite from magnetic and Mössbauer spectroscopic measurements. The M_s at room temperature is $\sim$59 Am^2kg^{-1} (3.13 μ_B/f.u.), which is much higher than previously published values because previous studies did not use high purity samples. The magnetic properties of the pure synthetic samples studied here are dominated by PSD/MD behavior, although traces of SP behavior are evident in ZFC/FC magnetization curves and in Mössbauer spectroscopic measurements. No low-temperature magnetic transition was detected, which confirms previous reports. However, a local coercivity minimum is clearly observed at around 130 K, which is probably related to the MD properties of the studied greigite samples. High-temperature magnetic analysis indicates that the synthetic samples start to undergo chemical decomposition at $\sim$250°C. High-temperature magnetic measurements on an extremely stable natural greigite sample indicate that the T_C of greigite must exceed 350°C, although the exact value of T_C remains unknown. The exchange constant of greigite was estimated using low-temperature M_s measurements. The mean spin wave stiffness value for greigite is estimated to be $\sim$193 meV·Å^2, with a corresponding exchange constant of $\sim$1.03 meV, which was obtained from the $T^{3/2}$ term of M_s based on the Bloch spin wave expansion. Further work is needed to check our estimated value of the exchange constant for greigite. Mössbauer spectroscopy indicates two magnetic sextets for octahedral and tetrahedral sites in greigite, which confirms previously reported hyperfine parameters for greigite (Table 2). These parameters increase with decreasing temperature and B_{eff} is higher for the octahedral sites than for the tetrahedral sites below room temperature.

[36] Production of pure greigite samples and new data presented here provide important new fundamental magnetic parameters for greigite. These determinations will benefit efforts to model magnetizations in a wide range of paleomagnetic and environmental magnetic studies of greigite-bearing sediments and also in studies of greigite magnetosomes in microorganisms.

[37] **Acknowledgments.** Liao Chang is supported by a Dorothy Hodgkin Postgraduate Award, funded by Hutchison Whampoa Limited and the U.K. Natural Environment Research Council. Greigite synthesis was supported by the National Natural Science Foundation of China (grants 20321101, 20125103 and 90206034). The Institute for Rock Magnetism, University of Minnesota (supported by the National Science Foundation Earth Sciences Division, the Keck Foundation and the University of Minnesota), provided a visiting fellowship that enabled partial completion of the magnetic and Mössbauer spectroscopic measurements. We thank Mike Jackson, Peat Sølheid, Amy Chen and Brian Carter-Stiglitz for help with measurements. The Institut Laue-Langevin, Grenoble, France is acknowledged for providing beam time for neutron diffraction experiments. We are grateful for constructive reviews from Mark Dekkers and an anonymous reviewer.

References

Aragón, R. (1992), Magnetization and exchange in nonstoichiometric magnetite, *Phys. Rev. B*, *46*, 5328–5333.

Babinszki, E., E. Marton, P. Marton, and L. F. Kiss (2007), Widespread occurrence of greigite in the sediments of Lake Pannon: Implications for environment and magnetostratigraphy, *Palaeogeogr. Palaeoclimatol. Palaeoecol.*, *252*, 626–636.

Bazylinski, D. A., B. R. Heywood, S. Mann, and R. B. Frankel (1993), Fe_3O_4 and Fe_3S_4 in a bacterium, *Nature*, *366*, 218.

Bazylinski, D. A., R. B. Frankel, B. R. Heywood, S. Mann, J. W. King, P. L. Donaghay, and A. K. Hanson (1995), Controlled biomineralization of magnetite (Fe_3O_4) and greigite (Fe_3S_4) in a magnetotactic bacterium, *Appl. Environ. Microbiol.*, *61*, 3232–3239.

Benning, L. G., R. T. Wilkin, and H. L. Barnes (2000), Reaction pathways in the Fe-S system below 100°C, *Chem. Geol.*, *167*, 25–51.

Berner, R. A. (1984), Sedimentary pyrite formation: An update, *Geochim. Cosmochim. Acta*, *48*, 605–615.

Bracci, G., D. Dalena, and P. Orlandi (1985), La greigite di Mentana, Lazio, *Bull. Mineral.*, *40*, 295–298.

Braga, M., S. K. Lie, C. A. Taft, and W. A. Lester Jr. (1988), Electronic structure, hyperfine interactions, and magnetic properties for iron octahedral sulfides, *Phys. Rev.*, *38*, 10,837–10,851.

Brockhouse, B. N., and H. Watanabe (1963), Spin waves in magnetite from neutron scattering, in *Inelastic Scattering of Neutrons in Solids and Liquids*, vol. 2, pp. 297–308, International Atomic Energy Agency Proceedings, Vienna.

Chang, L., A. P. Roberts, A. R. Muxworthy, Y. Tang, Q. W. Chen, C. J. Rowan, Q. S. Liu, and P. Pruner (2007), Magnetic characteristics of synthetic pseudo-single-domain and multi-domain greigite (Fe_3S_4), *Geophys. Res. Lett.*, *34*, L24304, doi:10.1029/2007GL032114.

Chen, X. Y., X. F. Zhang, J. X. Wan, Z. H. Wang, and Y. T. Qian (2005), Selective fabrication of metastable greigite (Fe_3S_4) nanocrystallites and its magnetic properties through a simple solution-based route, *Chem. Phys. Lett.*, *403*, 396–399.

Coey, J. M. D., M. R. Spender, and A. H. Morrish (1970), The magnetic structure of the spinel, Fe_3S_4, *Solid State Commun.*, *8*, 1605–1608.

de Boer, C. B., and M. J. Dekkers (1998), Thermomagnetic behaviour of haematite and goethite as a function of grain size in various non-saturating magnetic fields, *Geophys. J. Int.*, *133*, 541–552.

Dekkers, M. J. (1989), Magnetic properties of natural pyrrhotite. Part II: High- and low-temperature behaviour of J_{rs} and TRM as function of grain size, *Phys. Earth Planet. Inter.*, *57*, 266–283.

Dekkers, M. J., and M. A. A. Schoonen (1996), Magnetic properties of hydrothermally synthesized greigite. Part I: Rock magnetic parameters at room temperature, *Geophys. J. Int.*, *126*, 360–368.

Dekkers, M. J., H. F. Passier, and M. A. A. Schoonen (2000), Magnetic properties of hydrothermally synthesized greigite. Part II: High- and low-temperature characteristics, *Geophys. J. Int.*, *141*, 809–819.

Diaz-Ricci, J. C., and J. L. Kirschvink (1992), Magnetic domain state and coercivity predictions for biogenic greigite (Fe_3S_4): A comparison of theory with magnetosome observations, *J. Geophys. Res.*, *97*, 17,309–17,315.

Dunlop, D. J., and Ö. Özdemir (1997), *Rock Magnetism: Fundamentals and Frontiers*, 573 pp., Cambridge Univ. Press, Cambridge.

Farina, M., D. M. S. Esquivel, and H. G. P. Lins de Barros (1990), Magnetic iron-sulphur crystals from a magnetotactic microorganism, *Nature*, *343*, 256–258.

Fassbinder, J. W. E., and H. Stanjek (1994), Magnetic properties of biogenic soil greigite (Fe_3S_4), *Geophys. Res. Lett.*, *21*, 2349–2352.

Florindo, F., and F. Marra (1995), A revision of the stratigraphy for the Middle Pleistocene continental deposits of Rome (Central Italy): Palaeomagnetic data, *Ann. Geofis.*, *38*, 177–188.

Florindo, F., and L. Sagnotti (1995), Palaeomagnetism and rock magnetism in the upper Pliocene Valle Ricca (Rome, Italy) section, *Geophys. J. Int.*, *123*, 340–354.

Goodenough, J. B., and G. A. Fatseas (1982), Mössbauer ^{57}Fe isomer shift as a measure of valence in mixed-valence iron sulfides, *J. Solid State Chem.*, *41*, 1–22.

Greenwood, N. N., and T. C. Gibb (1971), *Mössbauer Spectroscopy*, 659 pp., CRC Press, Boca Raton, Fla.

He, Z. B., S. H. Yu, X. Y. Zhou, X. G. Li, and J. F. Qu (2006), Magnetic-field-induced phase-selective synthesis of ferrosulfide microrods by a hydrothermal process: Microstructure control and magnetic properties, *Adv. Funct. Mater.*, *16*, 1105–1111.

Heywood, B. R., S. Mann, and R. B. Frankel (1991), Structure, morphology and growth of biogenic greigite, *Mater. Res. Soc. Symp. Proc.*, *218*, 93–108.

Hilton, J. (1990), Greigite and the magnetic properties of sediments, *Limnol. Oceanogr.*, *35*, 509–520.

Hoffmann, V. (1992), Greigite (Fe_3S_4): Magnetic properties and first domain observations, *Phys. Earth Planet. Inter.*, *70*, 288–301.

Horiuchi, S., H. Wada, and T. Moori (1974), Morphology and imperfection of hydrothermally synthesized greigite (Fe_3S_4), *J. Cryst. Growth*, *24/25*, 624–626.

Hunger, S., and L. G. Benning (2007), Greigite: A true intermediate on the polysulfide pathway to pyrite, *Geochem. Trans.*, *8*, doi:10.1186/1467-4866-8-1.

Jiang, W. T., C. S. Horng, A. P. Roberts, and D. R. Peacor (2001), Contradictory magnetic polarities in sediments and variable timing of neoformation of authigenic greigite, *Earth Planet. Sci. Lett.*, *193*, 1–12.

Kasama, T., M. Pósfai, R. K. K. Chong, A. P. Finlayson, P. R. Buseck, R. E. Dunin-Borkowski, and R. B. Frankel (2006a), Magnetic microstructure of iron sulfide crystals in magnetotactic bacteria from off-axis electron holography, *Physica B*, *384*, 249–252.

Kasama, T., M. Pósfai, R. K. K. Chong, A. P. Finlayson, P. R. Buseck, R. B. Frankel, and R. E. Dunin-Borkowski (2006b), Magnetic properties, microstructure, composition, and morphology of greigite nanocrystals in magnetotactic bacteria from electron holography and tomography, *Am. Mineral.*, *91*, 1216–1229.

Keffer, F. (1966), Ferromagnetism, in *Encyclopedia of Physics*, vol. XVIII-2, edited by H. P. J. Wijn, 273 pp., Springer, New York.

Kenan, R. P., M. L. Glasser, and F. J. Milford (1963), Spin-wave contribution to the heat capacity of magnetite, *Phys. Rev.*, *132*, 47–49.

Kouvel, J. S. (1956), Specific heat of a magnetite crystal at liquid helium temperatures, *Phys. Rev.*, *102*, 1489–1490.

Krs, M., F. Novák, M. Krsová, P. Pruner, L. Koulíková, and J. Jansa (1992), Magnetic properties and metastability of greigite-smythite mineralization in brown-coal basins of the Krusné Hory Piedmont, Bohemia, *Phys. Earth Planet. Inter.*, *70*, 273–287.

Letard, I., Ph. Sainctavit, N. Menguy, J.-P. Valet, A. Isambert, M. Dekkers, and A. Gloter (2005), Mineralogy of greigite Fe_3S_4, *Phys. Scr.*, *T115*, 489–491.

Mann, S., N. H. C. Sparks, R. B. Frankel, D. A. Bazylinski, and H. W. Jannasch (1990), Biomineralization of ferrimagnetic greigite (Fe_3S_4) and iron pyrite (FeS_2) in a magnetotactic bacterium, *Nature*, *343*, 258–261.

Mattei, M., C. Kissel, and R. Funiciello (1996), No tectonic rotation of the Tuscan Tyrrhenian margin (Italy) since late Messinian, *J. Geophys. Res.*, *101*, 2835–2845.

Moskowitz, B. M., R. B. Frankel, and D. A. Bazylinski (1993), Rock magnetic criteria for the detection of biogenic magnetite, *Earth Planet. Sci. Lett.*, *120*, 283–300.

Nakazawa, H., and K. Sakaguchi (1972), Anhydrous synthesis of greigite, *Mineral. J.*, *6*, 458–463.

Néel, L. (1948), Propriétés magnétiques des ferrites: Ferrimagnétisme et antiferromagnétisme, *Ann. Phys.*, *3*, 137–198.

Néel, L. (1949), Théorie du traînage magnétique des ferromagnétiques en grains fins avec applications aux terres cuites, *Ann. Géophys.*, *5*, 99–136.

Opdyke, N. D., and J. E. T. Channell (1996), *Magnetic Stratigraphy*, 346 pp., Elsevier, New York.

Pearce, C. I., R. A. D. Pattrick, and D. J. Vaughan (2006), Electrical and magnetic properties of sulfides, *Rev. Mineral. Geochem.*, *61*, 127–180.

Pósfai, M., P. R. Buseck, D. A. Bazylinski, and R. B. Frankel (1998a), Iron sulfides from magnetotactic bacteria: Structure, composition, and phase transitions, *Am. Mineral.*, *83*, 1469–1481.

Pósfai, M., P. R. Buseck, D. A. Bazylinski, and R. B. Frankel (1998b), Reaction sequence of iron sulfide minerals in bacteria and their use as biomarkers, *Science*, *280*, 880–883.

Qian, X. F., X. M. Zhang, C. Wang, Y. Xie, W. Z. Wang, and Y. T. Qian (1999), The preparation and phase transition of nanocrystalline iron sulfides via toluene-thermal process, *Mater. Sci. Eng. B*, *64*, 170–173.

Radusinović, D. (1966), Greigite from the Lojane chromium deposit, Macedonia, *Am. Mineral.*, *51*, 209–215.

Reynolds, R. L., M. L. Tuttle, C. A. Rice, N. S. Fishman, J. A. Karachewski, and D. M. Sherman (1994), Magnetization and geochemistry of greigite-bearing Cretaceous strata, North Slope, Alaska, *Am. J. Sci.*, *294*, 485–528.

Rickard, D., and G. W. Luther III (2007), Chemistry of iron sulfides, *Chem. Rev.*, *107*, 514–562.

Roberts, A. P. (1995), Magnetic properties of sedimentary greigite (Fe_3S_4), *Earth Planet. Sci. Lett.*, *134*, 227–236.

Roberts, A. P., and G. M. Turner (1993), Diagenetic formation of ferrimagnetic iron sulphide minerals in rapidly deposited marine sediments, South Island, New Zealand, *Earth Planet. Sci. Lett.*, *115*, 257–273.

Roberts, A. P., and R. Weaver (2005), Multiple mechanisms of remagnetization involving sedimentary greigite (Fe_3S_4), *Earth Planet. Sci. Lett.*, *231*, 263–277.

Roberts, A. P., R. L. Reynolds, K. L. Verosub, and D. P. Adam (1996), Environmental magnetic implications of greigite formation in a 3 m.y. lake sediment record from Butte Valley, northern California, *Geophys. Res. Lett.*, *23*, 2859–2862.

Roberts, A. P., W. T. Jiang, F. Florindo, C. S. Horng, and C. Laj (2005), Assessing the timing of greigite formation and the reliability of the Upper Olduvai polarity transition record from the Crostolo River, Italy, *Geophys. Res. Lett.*, *32*, L05307, doi:10.1029/2004GL022137.

Roberts, A. P., Q. S. Liu, C. J. Rowan, L. Chang, C. Carvallo, J. Torrent, and C. S. Horng (2006), Characterization of hematite (α-Fe_2O_3), goethite (α-FeOOH), greigite (Fe_3S_4), and pyrrhotite (Fe_7S_8) using first-order reversal curve diagrams, *J. Geophys. Res.*, *111*, B12S35, doi:10.1029/2006JB004715.

Ron, H., N. R. Nowaczyk, U. Frank, M. J. Schwab, R. Naumann, B. Striewski, and A. Agnon (2007), Greigite detected as dominating remanence carrier in late Pleistocene sediments, Lisan Formation, from Lake Kinneret (Sea of Galilee), Israel, *Geophys. J. Int.*, *170*, 117–131.

Rowan, C. J., and A. P. Roberts (2006), Magnetite dissolution, diachronous greigite formation, and secondary magnetization from pyrite oxidation: Unravelling complex magnetizations in Neogene marine sediments from New Zealand, *Earth Planet. Sci. Lett.*, *241*, 119–137.

Sagnotti, L., and A. Winkler (1999), Rock magnetism and palaeomagnetism of greigite-bearing mudstones in the Italian Peninsula, *Earth Planet. Sci. Lett.*, *165*, 67–90.

Sagnotti, L., A. Winkler, L. Alfonsi, F. Florindo, and F. Marra (2000), Paleomagnetic constraints on the Plio-Pleistocene geodynamic evolution of the external central-northern Apennines (Italy), *Earth Planet. Sci. Lett.*, *180*, 243–257.

Schmidbauer, E., and M. Keller (2006), Magnetic hysteresis properties, Mössbauer spectra and structural data of spherical 250 nm particles of solid solutions Fe_3O_4 – γ-Fe_2O_3, *J. Magn. Magn. Mater.*, *297*, 107–117.

Schwarz, E. J., and D. J. Vaughan (1972), Magnetic phase relations of pyrrhotite, *J. Geomagn. Geoelectr.*, *24*, 441–458.

Skinner, B. J., R. C. Erd, and F. S. Grimaldi (1964), Greigite, the thiospinel of iron; A new mineral, *Am. Mineral.*, *49*, 543–555.

Snowball, I. F. (1991), Magnetic hysteresis properties of greigite (Fe_3S_4) and a new occurrence in Holocene sediments from Swedish Lappland, *Phys. Earth Planet. Inter.*, *68*, 32–40.

Snowball, I. F., and R. Thompson (1988), The occurrence of greigite in sediments from Loch Lomond, *J. Quat. Sci.*, *3*, 121–125.

Snowball, I. F., and R. Thompson (1990), A stable chemical remanence in Holocene sediments, *J. Geophys. Res.*, *95*, 4471–4479.

Spender, M. R., J. M. D. Coey, and A. H. Morrish (1972), The magnetic properties and Mössbauer spectra of synthetic samples of Fe_3S_4, *Can. J. Phys.*, *50*, 2313–2326.

Srivastava, C. M., and R. Aiyar (1987), Spin wave stiffness constants in some ferrimagnetics, *J. Phys. Condens. Matter*, *20*, 1119–1128.

Tang, Y., Q. W. Chen, Y. Xiong, and Y. Li (2007), Magnetic field-induced increase in conversion rate of Fe_3S_4 to FeS_2, *Chin. J. Inorg. Chem.*, *23*, 941–947.

Tric, E., C. Laj, C. Jéhanno, J.-P. Valet, C. Kissel, A. Mazaud, and S. Iaccarino (1991), High-resolution record of the Upper Olduvai transition from Po Valley (Italy) sediments: Support for dipolar transition geometry?, *Phys. Earth Planet. Inter.*, *65*, 319–336.

Uda, M. (1965), On the synthesis of greigite, *Am. Mineral.*, *50*, 1487–1489.

Vandenberghe, R. E., E. De Grave, P. M. A. De Bakker, M. Krs, and J. J. Hus (1991), Mössbauer effect study of natural greigite, *Hyperfine Interact.*, *68*, 319–322.

van Dongen, B. E., A. P. Roberts, S. Schouten, W. T. Jiang, F. Florindo, and R. D. Pancost (2007), Formation of iron sulfide nodules during anaerobic oxidation of methane, *Geochim. Cosmochim. Acta*, *71*, 5155–5167.

Vasiliev, I., M. J. Dekkers, W. Krijgsman, C. Franke, C. G. Langereis, and T. A. T. Mullender (2007), Early diagenetic greigite as a recorder of the palaeomagnetic signal in Miocene-Pliocene sedimentary rocks of the Carpathian foredeep (Romania), *Geophys. J. Int.*, *171*, 613–629.

Vaughan, D. J., and J. A. Tossell (1981), Electronic structure of thiospinel minerals: Results from MO calculations, *Am. Mineral.*, *66*, 1250–1253.

Verwey, E. J. W. (1939), Electronic conduction of magnetite (Fe_3O_4) and its transition point at low temperatures, *Nature*, *144*, 327–328.

Yamaguchi, S., and T. Katsurai (1960), Zur Bildung des ferromagnetischen Fe_3S_4, *Kolloid Zeit.*, *170*, 147–148.

Yamaguchi, S., and H. Wada (1969), Zum hydrothermal synthetisierten eisen-Thiospinell, *Naturwissenschaften*, *56*, 138.

Yamaguchi, S., and H. Wada (1970), Magnetic anisotropy of Fe_3S_4 as revealed by electron diffraction, *J. Appl. Phys.*, *41*, 1873–1874.

L. Chang and A. P. Roberts, National Oceanography Centre, University of Southampton, European Way, Southampton SO14 3ZH, UK. (changl@noc.soton.ac.uk)

Q. Chen and Y. Tang, Hefei National Laboratory for Physical Sciences at Microscale and Department of Materials Science and Engineering, University of Science and Technology of China, Hefei 230026, China.

A. R. Muxworthy, Department of Earth Science and Engineering, Imperial College London, South Kensington Campus, London SW7 2AZ, UK.

B. D. Rainford, School of Physics and Astronomy, University of Southampton, Southampton SO17 1BJ, UK.